THE JOURNAL OF BIOLOGICAL CHEMISTRY VOL. 289, NO. 34, pp. 23276–23286, August 22, 2014

Crystal Structure and Site-directed Mutational Analysis Reveals Key Residues Involved in *Escherichia coli* ZapA Function*

Received for publication, February 27, 2014, and in revised form, July 3, 2014 Published, JBC Papers in Press, July 7, 2014, DOI 10.1074/jbc.M114.561928

Elyse J. Roach, Matthew S. Kimber, and Cezar M. Khursigara[1]

From the Department of Molecular and Cellular Biology, University of Guelph, Guelph, Ontario N1G 2W1, Canada

Background: ZapA and FtsZ interact prior to bacterial cell division to stabilize the Z-ring.
Results: The structure of *E. coli* ZapA reveals a charged α-helix important for FtsZ interactions.
Conclusion: Key residues in the charged α-helix of ZapA are important for FtsZ filament bundling.
Significance: ZapA facilitates FtsZ filament bundling and Z-ring stability in dividing bacterial cells.

FtsZ is an essential cell division protein in *Escherichia coli*, and its localization, filamentation, and bundling at the mid-cell are required for Z-ring stability. Once assembled, the Z-ring recruits a series of proteins that comprise the bacterial divisome. Zaps (FtsZ-associated proteins) stabilize the Z-ring by increasing lateral interactions between individual filaments, bundling FtsZ to provide a scaffold for divisome assembly. The x-ray crystallographic structure of *E. coli* ZapA was determined, identifying key structural differences from the existing ZapA structure from *Pseudomonas aeruginosa*, including a charged α-helix on the globular domains of the ZapA tetramer. Key helix residues in *E. coli* ZapA were modified using site-directed mutagenesis. These ZapA variants significantly decreased FtsZ bundling in protein sedimentation assays when compared with WT ZapA proteins. Electron micrographs of ZapA-bundled FtsZ filaments showed the modified ZapA variants altered the number of FtsZ filaments per bundle. These *in vitro* results were corroborated *in vivo* by expressing the ZapA variants in an *E. coli* Δ*zapA* strain. *In vivo*, ZapA variants that altered FtsZ bundling showed an elongated phenotype, indicating improper cell division. Our findings highlight the importance of key ZapA residues that influence the extent of FtsZ bundling and that ultimately affect Z-ring formation in dividing cells.

Bacterial cell division requires the presence, accumulation and mid-cell localization of FtsZ (filamentous temperature-sensitive protein Z). FtsZ is a 40-kDa monomeric protein with GTPase activity that shows structural and functional homology to the eukaryotic protein tubulin (1–5). FtsZ binds and hydrolyzes GTP *in vivo* (6) and also polymerizes to form the Z-ring at mid-cell. The Z-ring forms prior to cell division and acts as a scaffold for the recruitment of all downstream cell division proteins; together these comprise the "divisome" (7–10). In *Escherichia coli*, the divisome includes ~20 essential and nonessential proteins (11–13). Divisome proteins are recruited in a hierarchal manner and depend on the Z-ring for stability. Included in the divisome are the Zaps (FtsZ-associated proteins): ZapA, ZapB, ZapC, and ZapD (14–19). These Zaps stabilize the Z-ring by increasing lateral interactions between individual filaments, thus bundling FtsZ to provide a scaffold for divisome assembly (9, 20).

Our knowledge of the functional, structural, and biochemical significance of the Zaps in *E. coli* is limited. It has been demonstrated that they are not individually essential *in vivo* (14, 15, 17). However, because of their potentially overlapping function and temporal recruitment to the Z-ring, it may be the cooperative interaction of all four proteins with FtsZ that has a significant impact on cell division (14, 15). Advances in microscopy have aided in the visualization of FtsZ filaments *in vitro* (5, 21–25) and Z-ring formation *in vivo* (2, 26–30). Depending on the techniques and bacterial species used, recent superresolution fluorescence studies suggest that, *in vivo*, FtsZ filaments may adopt either a dynamic "bead-like" organization (31); loose, overlapping bundles comprised of multiple FtsZ filaments (30, 32); loosely packed continuous bands of bundled FtsZ filaments (33); or a combination of the arrangements described above (34, 35). Although ZapA and ZapB have been implicated in positioning FtsZ protofilaments at mid-cell (30), the precise function of the Zap proteins *in vivo* remains unclear.

ZapA has been shown to bundle FtsZ *in vitro*, and ZapA-deficient strains exhibit significant elongation, indicating a cell division defect (14, 30, 36, 37). To date, all biochemical studies on the *E. coli* ZapA protein (*Ec*ZapA)[2] have been interpreted in the context of the crystal structure of the tetrameric *Pseudomonas aeruginosa* ZapA (*Pa*ZapA) (37–40). Because these two proteins share only 25% sequence identity (as determined by ClustalW (41)), a structure of *E. coli* ZapA may aid in advancing understanding about the lateral interactions that bundle FtsZ filaments. Recently, a critical region on *E. coli* ZapA was identified by a bacterial two-hybrid assay (36). This 26-amino acid region is weakly conserved across bacterial species but contains

* This work was funded by Natural Sciences and Engineering Research Council of Canada Discovery Grants 371639 (to C. M. K.) and 327280 (to M. S. K.).
The atomic coordinates and structure factors (code 4P1M) have been deposited in the Protein Data Bank (http://wwpdb.org/).

[1] To whom correspondence should be addressed: Dept. of Molecular and Cellular Biology, University of Guelph, 50 Stone Rd. E, Guelph, Ontario N1G 2W1, Canada. Tel.: 519-821-4120, Ext. 58091; Fax: 519-837-1802; E-mail: ckhursig@uoguelph.ca.

[2] The abbreviations used are: *Ec*ZapA, *E. coli* ZapA; *Pa*ZapA, *P. aeruginosa* ZapA; r.m.s.d., root mean square deviation; TEM, transmission electron microscopy.

TABLE 1
Strains, plasmids, and primers used in this study

	Description/genome/sequence	Source
***E. coli* strains**		
DH5α	F$^-$ *endA1 glnV44 thi-1 recA1 relA1 gyrA96 deoR nupG* Φ80d*lacZ*ΔM15Δ (*lacZYA-argF*)U169, *hsdR17* (r_K^- m_K^+), λ−	Invitrogen
BL21(DE3)	F$^-$ *ompT gal dcm lon hsdS*$_B$(r_B^- m_B^-) λ(DE3) pLysS(cm^R)[a]	New England Biolabs
W3110	*rph-1*IN (*rrnD-rrnE*)	Coli Genetic Stock Centre
Δ*zapA*	W3110, Δ*zapA*	This work
Plasmids		
pEJR005b	Modified pET28A (no histidine tag) with WT *ftsZ* from *E. coli*	This work
pEJR029b	pBAD24 with WT His_6-*zapA* from *E. coli*	This work
pEJR029b_D22A	pBAD24 with D22A His_6-*zapA* from *E. coli*	This work
pEJR029b_R24A	pBAD24 with R24A His_6-*zapA* from *E. coli*	This work
pEJR029b_N28A	pBAD24 with N28A His_6-*zapA* from *E. coli*	This work
pEJR029b_D32A	pBAD24 with D32A His_6-*zapA* from *E. coli*	This work
pEJR029b_D33A	pBAD24 with D33A His_6-*zapA* from *E. coli*	This work
pEJR029b_D33K	pBAD24 with D33K His_6-*zapA* from *E. coli*	This work
pEJR029b_R46A	pBAD24 with R46A His_6-*zapA* from *E. coli*	This work
Primers for mutagenesis		
D22A_F	5′-AACTGCCCGCCTGCCCAAAGGGATGCG-3′	This work
D22A_R	5′-CGCATCCCTTTGGGCAGGCGGGCAGTT-3′	This work
R24A_F	5′-GAACTGCCCGCCTGACCAAGCGGATGCGTTGAATC-3′	This work
R24A_R	5′-GATTCAACGCATCCGCTTGGTCAGGCGGGCAGTTC-3′	This work
N28A_F	5′-CCAAAGGGATGCGTTGGCTCAGGCAGCGGACGAT-3′	This work
N28A_R	5′-ATCGTCCGCTGCCTGAGCCAACGCATCCCTTTGG-3′	This work
D32A_F	5′-TGAATCAGGCAGCGGCCGATCTGAACCAACG-3′	This work
D32A_R	5′-CGTTGGTTCAGATCGGCCGCTGCCTGATTCA-3′	This work
D33A_F	5′-CAGGCAGCGGACGCTCTGAACCAACGG-3′	This work
D33A_R	5′-CCGTTGGTTCAGAGCGTCCGCTGCCTG-3′	This work
D33K_F	5′-GAATCAGGCAGCGGACAAGCTGAACCAACGGTTGC-3′	This work
D33K_R	5′-GCAACCGTTGGTTCAGCTTGTCCGCTGCCTGATTC	This work
R46A_F	5′-GGTTGCAAGATCTGAAAGAACGCACTGCAGTCACAAATACTGAA-3′	This work
R46A_R	5′-TTCAGTATTTGTGACTGCAGTGCGTTCTTTCAGATCTTGCAACC-3′	This work

[a] cm^R, chloramphenicol resistance.

several charged residues that could potentially interact with FtsZ. Here, we report the crystal structure of the *Ec*ZapA tetramer showing several key differences from its *P. aeruginosa* counterpart. Additionally, by targeting charged amino acids on the α-helix of the N-terminal globular domain of *Ec*ZapA, we have identified key residues involved in the ZapA-FtsZ interaction that promote filament bundling.

EXPERIMENTAL PROCEDURES

Cloning, Site-directed Mutagenesis, and Construction of Zap Deletion Strain—Plasmids containing *zapA* and *ftsZ* were constructed by amplifying the *zapA* and *ftsZ* genes using primers 308F (TATATGAATTCATGCACCACCACCACCACCACAGCATCGAAGGTCGAAGTGGTATGTCTGCACAACCCGGTCGATATC) and 308R (TATCGAAGCTTTCATTCAAAGTTTTGGTTAGTTTTTTCGGTGATGCGACCTTGTTCAAGTAACGCTTGTTCTATGG), and 400F (TTTAATACCATGGTGTTTGAACCAATGGAACTTACCAATG) and 400R (TATTATAAGCTTTTATTAATCAGCTTGCTTACGCAGGAATG), respectively. The *zapA* gene from *E. coli* W3110 was amplified and cloned into pBAD24 as an EcoRI-HindIII His tag-encoding fragment (sites underlined). The *ftsZ* gene was cloned into pET28a using the NcoI and HindIII cut sites (sites underlined) so as to exclude the plasmid-encoded His tag. The Δ*zapA* strain was made using the λ red deletion system as described previously (42, 43). The entire *zapA* gene was replaced with the *cat* region from pKD3 mediated by the λ red operon products from pSIM6 in *E. coli* DH5α. Site-directed mutagenesis was performed using the QuikChange® Lightning site-directed mutagenesis kit (Stratagene), and *zapA* variant sequences were amplified using the primers listed in Table 1.

Protein Expression and Purification—FtsZ expression was induced by the addition of 1 mM isopropyl 1-thio-β-D-galactopyranoside (Roche) in an *E. coli* BL21(DE3) pLysS strain at 37 °C for 3 h in LB medium supplemented with kanamycin and chloramphenicol. Cell pellets were resuspended in PEM-KOH buffer (50 mM piperazine-*N*,*N*′-bis(ethanesulfonic acid)-KOH, 1 mM EDTA, 5 mM $MgCl_2$, pH 6.5) and lysed by French press. Cell debris was removed by centrifugation at 8,000 × *g* for 15 min, and membranes were removed by centrifugation at 100,000 × *g* for 1 h. FtsZ was purified by two rounds of calcium cycling as described previously (23) with an additional low speed centrifugation step (8,000 × *g* for 5 min) before desalting using Amicon® Ultra-15 10,000 NMWL centrifugal filters (Millipore). FtsZ was then stored at 4 °C for no longer than 4 days in PEM-KOH buffer. For His_6-ZapA expression, an overnight culture of *E. coli* BL21(DE3) pLysS cells carrying the pEJR029b plasmid was diluted 1/100 into LB medium supplemented with ampicillin. Cells were grown at 37 °C to an A_{600} of 1.0 (~2 h) and then induced by the addition of 0.2% (v/v) L-arabinose (Sigma). Expression proceeded for 1 h before cell pellets were collected by centrifugation. After pelleting, cells were resuspended in A1 buffer (20 mM Tris, 50 mM NaCl, 20 mM imidazole, pH 7.4) and lysed by French press. Cell debris and membranes were removed as described for FtsZ (above). His_6-ZapA was purified by immobilized metal affinity chromatography, using the Biologic™ Duoflow Chromatography System (Bio-Rad). Soluble protein fractions were loaded onto an MT2 column (Bio-Rad) packed with nickel-nitrilotriacetic acid Superflow resin (Qiagen). After washing with six column volumes of A1 buffer containing 75 mM imidazole, His_6-ZapA was eluted

with a linear gradient of imidazole from 75–500 mM. His_6-ZapA fractions were pooled, concentrated, and desalted using Amicon® Ultra-15 3,000 NMWL centrifugal filters (Millipore). Purified His_6-ZapA was stored at 4 °C in A1 buffer for no longer than 4 weeks with no loss of activity during this period.

Crystallization, Data Collection, Structure Determination, and Analysis of ZapA—We crystallized *Ec*ZapA from 0.5 M ammonium sulfate, 1.0 M lithium sulfate, and 0.1 M sodium citrate, pH 5.6. Crystals grew as hexagonal bipyramids up to 500 μm in length. After the removal of surface water by immersion in paratone N-oil, crystals were frozen in liquid nitrogen. The data were collected at the Canadian Synchrotron Light Source (the Canadian Macromolecular Crystallography Facility, Beamline 08ID-1) and processed in XDS (44). Initial attempts at molecular replacement failed in Phaser (45) with a variety of search models derived from the *Pa*ZapA dimer or protomer. Molecular replacement eventually succeeded with a single protomer search model, comprising residues 50–94. This model comprises less than 25% of the asymmetric unit, with a pairwise sequence identity of only ~30% to the target. The top translation function scores for the second copy just exceeded the Z-score of 8.0, which generally indicates a reliable molecular replacement solution. The solution is actually out of sequence register with respect to the final model and with different offsets in the two protomers. The C-terminal helix appears to act as a generic α-helical model of approximately the correct curvature, capturing the essential structural elements independent of the underlying sequence. This initial model was subjected to autobuild in Phenix (46), which was able to correctly build most of chain A. The rest of the structure was completed manually by rebuilding in Coot (47) and refined in Phenix (46), using a translation-liberation-screw model of the atomic displacement parameters.

FtsZ Filamentation and Sedimentation Assays—FtsZ (4.8 μM) filamentation was performed in PEM-KOH buffer at 30 °C upon the addition of GTP to 1 mM; in all cases samples were preincubated for 5 min at 30 °C before filamentation. Sedimentation assays were performed by titrating His_6-ZapA (0.5, 1.0, 2.1, 4.8, 8.1, and 11.4 μM) against a constant concentration of FtsZ (4.8 μM). His_6-ZapA and FtsZ were diluted and mixed in PEM-KOH buffer, GTP was added to 1 mM (with the exception of the negative control), and reactions were incubated at 30 °C for 5 min. Following incubation, an aliquot of total protein was taken from each reaction and mixed with 5× SDS sample buffer for analysis. Samples were sedimented at 10,000 rpm for 15 min. Previous studies (36, 40) used 80,000 rpm for 10 min to sediment FtsZ-ZapA bundles, and we observed no differences in FtsZ-ZapA sedimentation between these conditions (data not shown). Soluble protein was obtained from the supernatant, whereas pellets were resuspended in an equal volume of PEM-KOH buffer; both were mixed with 5× SDS sample buffer for analysis. All protein samples were boiled in sample buffer and analyzed by SDS-PAGE followed by Coomassie Blue staining using the SimplyBlue™ SafeStain (Invitrogen). We performed densitometry on gels to determine the amounts of soluble and pelleted FtsZ relative to the total protein fractions from each reaction using ImageLab™ Software (Bio-Rad). Pellet fractions were compared with the initial fraction, which was set to 100%. To account for FtsZ pelleting out of solution when not bundled, control reactions were performed containing FtsZ and the ZapA variant alone, without GTP. This amount of pelleting was then subtracted from all other pellet values. Additionally, FtsZ filamented by GTP was pelleted as a control to be sure that unbundled filaments did not pellet out of solution when centrifuged at this speed.

In Vivo Complementation and Immunofluorescence—Chemically competent *E. coli* Δ*zapA* cells were made by standard methods. Each pBAD24 vector containing mutated *zapA* (Table 1) was transformed into these cells, after which a single colony was chosen and grown for 16 h. Cultures were then diluted 1/100 in LB medium and allowed to grow to an A_{600} of 1.0. Expression was then induced by the addition of L-arabinose to 0.1% (w/v). Cells were adhered to a copper 200 mesh electron microscopy grid (Canemco) and imaged by transmission electron microscopy. For each variant, ~20 random fields of view were imaged, and >100 cells from two experimental replicates were measured using ImageJ (48). Immunofluorescence was performed as described by Hiraga *et al.* (49) with minor modifications. Cells were prepared and fixed as described previously. Cells were then blocked with 10% normal goat serum (Invitrogen) for 30 min at room temperature. The blocking solution was replaced with primary antibody (1:100 rabbit anti-FtsZ (Cedarlane) in 1% (w/v) BSA-PBST; PBS with 0.05% (v/v) Tween 20). Slides were incubated for 1 h at room temperature before removing the primary antibody and washing with PBST. Secondary antibody (1:200 goat anti-rabbit conjugated to FITC (Sigma-Adrich) in 1% (w/v) BSA-PBST) was added and incubated for 1 h at room temperature. Secondary antibody was removed, and samples were washed with PBST; samples were counterstained with 4′,6-diamidino-2-phenylindole (10 μg/ml) for 1 min in the dark and washed with PBST. Coverslips were mounted on the slides with SlowFade® Gold antifade reagent (Invitrogen). The slides were imaged using a Leica DM5000B fluorescent microscope equipped with a Hamamatsu ImagEM EM-CCD digital camera (Quorum Technologies). Images were analyzed using Volocity software (version 6.3; PerkinElmer Life Sciences).

Transmission Electron Microscopy (TEM)—For protein filaments and bundles, grids were subjected to 7 s of plasma cleaning in the Solarus™ advanced plasma cleaning system (Gatan). Protein samples were adhered to the grid for 45 s, washed once with PEM-KOH buffer and once with double distilled H_2O, then stained with 2% uranyl acetate for 30 s, and allowed to air dry. For whole cell samples, cells were adhered to a copper grid for 10 s, stained with 1% uranyl acetate for 7 s, then washed once with double distilled H_2O, and allowed to air dry. Grids were imaged using the FEI Tecnai G2 F20 operated at 120 kV.

RESULTS

X-ray Crystallographic Structure of E. coli ZapA (EcZapA)—*Ec*ZapA was determined to a resolution of 1.95 Å (Fig. 1 and Table 2), with two molecules per asymmetric unit. N-terminal residues 1–3 in chain A are disordered, whereas residues 1 and 46 in chain B are too poorly defined to reliably model. Similar to *Pa*ZapA (38), the structure is organized into two distinct domains, with the first 49 residues forming a globular domain

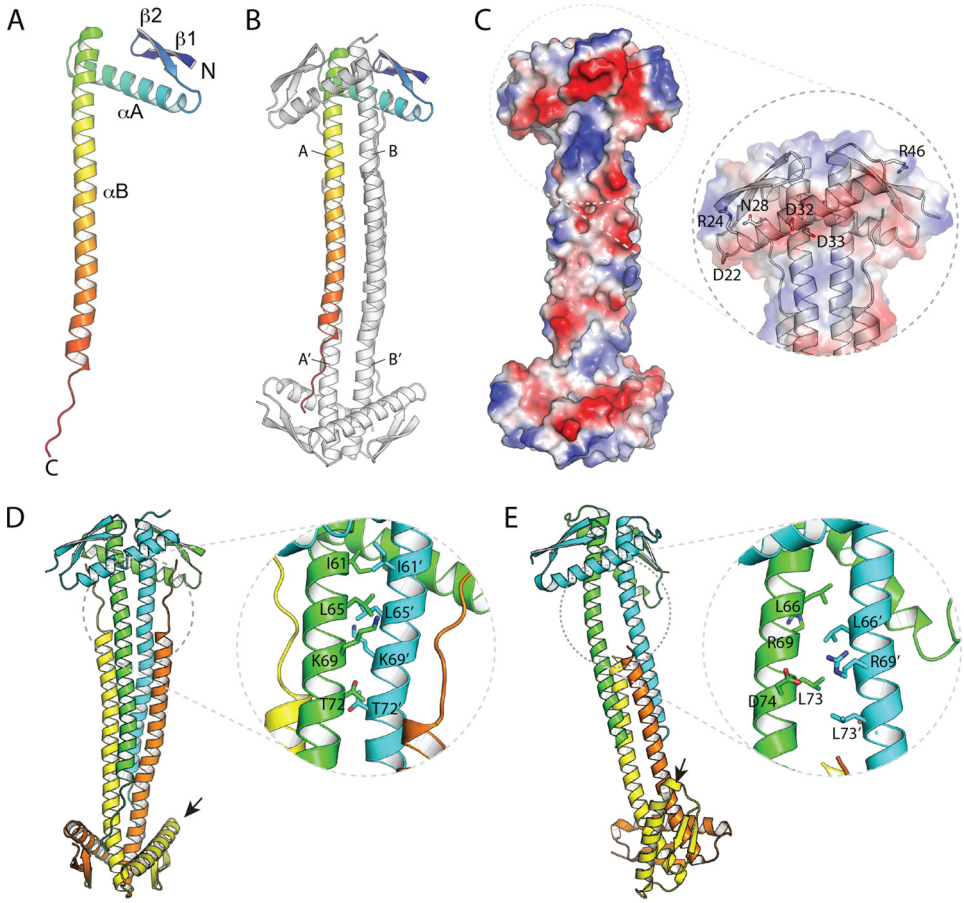

FIGURE 1. **X-ray crystallographic structure of *E. coli* ZapA.** *A*, the *Ec*ZapA protomer is organized as a compact N-terminal domain, with an extended C-terminal tail that is built as a single, elongated α-helix. *B*, the *Ec*ZapA tetramer is comprised of two protomers that form a tight dimer, mediated mostly by coiled-coil-like interactions between the long αB helix. This dimer interacts through the C-terminal end of this α-helix to form a four-helix bundle. Chain identities referred to in the text are marked. *C*, the electrostatic surface of the *Ec*ZapA tetramer highlights the N-terminal α-helix, αA, which forms a prominent ridge of electronegative residues. The *inset* shows the cartoon representation, as well as residues chosen for more detailed studies. *D* and *E*, details in the packing of the *Ec*ZapA tetramer (*D*) *versus* packing in the *Pa*ZapA tetramer (*E*). Note that the two structures were oriented by superimposing the upper dimer of the structure. Although the structures do bear an overall resemblance, they differ in numerous details. In particular, the interactions between protomers of the tight dimer are very different, with *Ec*ZapA using a coiled-coil interaction, whereas *Pa*ZapA has a ladder of hydrophobic residues that interdigitate. In the latter case, this results in the two protomers of the dimer having a noticeable vertical offset from one another. The N-terminal domains also differ markedly in their orientation relative to the C-terminal helices. In *Ec*ZapA, the N-terminal domains both sit at a similar angle across the two C-terminal helices. In *Pa*ZapA, one N-terminal domain in each dimer shows a marked shift and interacts with αB at an acute angle. Differences in packing of the helical domains also result in the N-terminal domains at opposite ends of the dimer aligning to the same face in *Ec*ZapA but rotated almost 90° around the long axis in *Pa*ZapA (*small arrows*).

comprised of a two stranded antiparallel β-sheet plus an α-helix, whereas the C-terminal half of the protein (residues 50–102) forms a single, 14-turn α-helix. The ZapA protomer is organized into a pseudosymmetric tetramer, where chains A and B interact with their doppelgangers A′ and B′ through a crystallographic 2-fold axis (Fig. 1, *B* and *C*). The strongest interaction forms a tight dimer that is stabilized predominantly by interactions mediated by the long C-terminal helix. In *Ec*ZapA, the first seven turns of the two helices interact through a coiled-coil type packing arrangement, where the two helices wrap around one another to form a left-handed superhelix; the two helices therefore cross at a 20° angle, and equivalent residues pack against one another laterally. Interactions are also mediated by the N-terminal domains, which pack against both helices so that both the α-helix and β-strands pack onto the second protomer. Note that the two chains of *Ec*ZapA differ significantly, with an r.m.s.d. of 2.0 Å; this difference is mostly attributable to significant differences in the twist of the C-terminal helices of the respective chains required to optimize these interactions. Overall, the tight dimer interface (A to B) buries 1670 Å^2 per protomer (Fig. 1*B*). The distal ends of the C-terminal helices splay apart from their dimeric mates, packing instead against the other dimer in a four-helix bundle-like arrangement. Residues 103–109, C-terminal to this helix, are also all ordered. They pack in an extended conformation against the C-terminal helix from a related protomer, with the last two residues of the protein interacting with the N-terminal domain of the opposite dimer. The tetramer is stabilized by burying ~1500 Å^2 per protomer between A and A′ (and also B and B′) and a further 920 Å^2 between symmetry-related copies of chains A and B′ (as well as B and A′). PISA predicts that the dissociation energy of the tetramer (−54.0 kcal/mol) is larger than the combined dissociation energy of the respective dimers (−28.6 kcal/mol).

Despite an overall resemblance to the *Pa*ZapA structure, the *EcZapA* structure differs in many important aspects (Fig. 1, *D versus E*). The C-terminal helix of *Pa*ZapA exhibits much less extensive interaction between tetramers than *Ec*ZapA (five

TABLE 2
Data collection, model refinement, and final structure statistics for *Ec*ZapA

Space group	$P6_122$
Cell dimensions	
$a = b$	54.10 Å
c	328.07 Å
Wavelength (Å)	0.97949
Resolution (Å)	50-1.95
Total observations	200,730
Unique observations	22,080
Completeness (last shell)[a]	0.999 (0.999)
$<I/\sigma(I)>$ (last shell)[a]	19.4 (2.7)
R_{sym} (last shell)[a]	0.067 (0.84)
Asymmetric unit contents	
Protein chains	2
Water molecules	118
Other molecules	1 Cl^-
Average B-factor (Å^2)	
Protein	51.8
Water	45.8
R_{cryst}	0.224
R_{free}[b]	0.27
r.m.s.d. bond lengths (Å)	0.006
r.m.s.d. bond angles (°)	0.996
Ramachandran plot[c]	
Favored (%)	98.6
Disallowed (%)	0.5

[a] The last shell includes all reflections between 2.00 and 1.95 Å.
[b] R_{free} calculated using 5% of the data, which were chosen randomly.
[c] Calculated using Molprobity.

turns of helix *versus* nine). This may have functional implications, because the *Pa*ZapA tetramer seems capable of dissociating into a dimer. In addition, the C-terminal residues in *Pa*ZapA are disordered, and so do not form the extended interactions seen in *Ec*ZapA. The interactions between protomers within the dimer are also fundamentally different in *Pa*ZapA. In the *Pa*ZapA structure, the C-terminal helices pack in parallel, but with the helices offset by one turn, so that each residue packs above the equivalent one (Fig. 1*E*). The offset of the two C-terminal helices presents two different interaction surfaces to the N-terminal domain, which then packs into two clearly distinct conformations differing by a large (~40°) rotation. Together, these differences in protomer orientation result in dimers that are structurally different from those in the *Ec*ZapA structure (Fig. 1*D*) and whose protomers superpose with an r.m.s.d. of 5.7 Å (a difference more typically seen between two proteins that are almost at the limits of detectable relatedness). Note that this asymmetry is seen in two independent structures (Protein Data Bank codes 1T3U and 1W2E) in different crystal forms (38) and are highly unlikely to represent an artifact of crystal packing.

ZapA Variants Show Altered FtsZ Bundling Capability in Vitro—Galli and Gerdes (36) reported that the N-terminal domain of *E. coli* ZapA alone was capable of interacting with FtsZ, albeit weakly (36). Based on their bacterial two-hybrid assay results, we mutated six residues of ZapA (Fig. 1*C*, *inset*, and Table 1) to assess their roles in ZapA interactions with FtsZ filaments.

ZapA is proposed to bundle FtsZ by increasing the lateral interactions between filaments (14, 36, 38, 50, 51). This bundling interaction can be studied *in vitro* using a sedimentation assay. In the presence of ZapA, FtsZ filaments come out of solution, whereas in the absence of ZapA, they remain soluble (36, 40). This approach was used to titrate the sedimentation of FtsZ filaments using WT ZapA and ZapA variants generated by site-directed mutagenesis (Table 1) along the charged N-terminal α-helix (Fig. 1*C*, *inset*). First, FtsZ was allowed to form filaments in the absence of ZapA, as a control, to ensure proper filament formation (Fig. 2*A*). These FtsZ filaments resemble those described previously (3, 51) and are single filaments ~5 nm in width ($n = 100$). Next, ZapA variants were mixed at subequimolar (0.5, 1.0, and 2.1 μM), equimolar (4.8 μM; Fig. 2*B*) (46), and saturated concentrations (8.1 μM and 11.4 μM) with a constant concentration of FtsZ, and filament sedimentation was monitored by SDS-PAGE (Fig. 2*C*). The sedimentation assays presented in this study were conducted at pH 6.5 as previously described (14, 36, 37, 40, 50, 51). However, FtsZ-ZapA bundles have also been reported at the more physiologically relevant pH of 7.5 (50). For each reaction, the initial ZapA-FtsZ mixture was incubated for 2 min and centrifuged to separate the soluble and pellet fractions (Fig. 2*C*). These experiments were performed in triplicate, and the pelleted fractions were analyzed by densitometry (Fig. 2*D*). For WT ZapA, filamentous FtsZ sedimentation increases with increasing ZapA concentration until equimolar concentrations (Fig. 2*C*). At 0.5 μM WT ZapA sediments ~16% of FtsZ filaments in solution compared with ~86% at the physiologically relevant equimolar concentration of 4.8 μM (46). When saturated with ZapA (11.4 μM), ~87% of FtsZ filaments are found in the pellet; this indicates that, at equimolar concentrations, WT ZapA can sufficiently sediment the majority of FtsZ filaments. As residues along the charged helix are altered (Fig. 1*C*, *inset*), clear differences emerge in the ability of the ZapA variants to pellet FtsZ, most notably at equimolar and saturated concentrations (Fig. 2*C*). For example, at equimolar concentrations N28A shows a 73% decrease in FtsZ sedimentation compared with WT ZapA (Fig. 2*C*). We also generated a D40A ZapA variant, but this construct did not express in *E. coli* cells, and we were not able to purify it. This result is similar to what Pacheco-Gómez *et al.* (40) reported with mutational analysis of residue 41 of *E. coli* ZapA, indicating that these residues may be critical for ZapA expression and proper protein folding *in vivo*.

To better visualize the differences observed in the sedimentation assays, we plotted the densitometric data as ZapA concentration *versus* the proportion of FtsZ filaments sedimented (Fig. 2*D*). The sedimentation profile of the D22A ZapA variant closely resembles WT ZapA. However, clear differences are seen in the ability of the other ZapA variants to bundle and sediment FtsZ filaments (Fig. 2*D*). R24A ZapA exhibits a clear shift when compared with WT ZapA, indicating that a higher concentration of this variant is required to initiate FtsZ sedimentation. D33A ZapA reaches maximal FtsZ filament pelleting at equimolar concentrations, similar to WT ZapA; however, the maximum proportion of FtsZ pelleted here is much lower than for WT. In contrast, ZapA variants N28A, D32A, D33K, and R46A show differences in both the amount of ZapA protein required to initiate sedimentation of FtsZ filaments and maximal FtsZ filament sedimentation. The most pronounced differences compared with WT are seen with D33A and N28A ZapA variants. ZapA D33A reveals the lowest FtsZ sedimentation at the saturated concentrations, and N28A ZapA shows the lowest FtsZ sedimentation at equimolar concentrations.

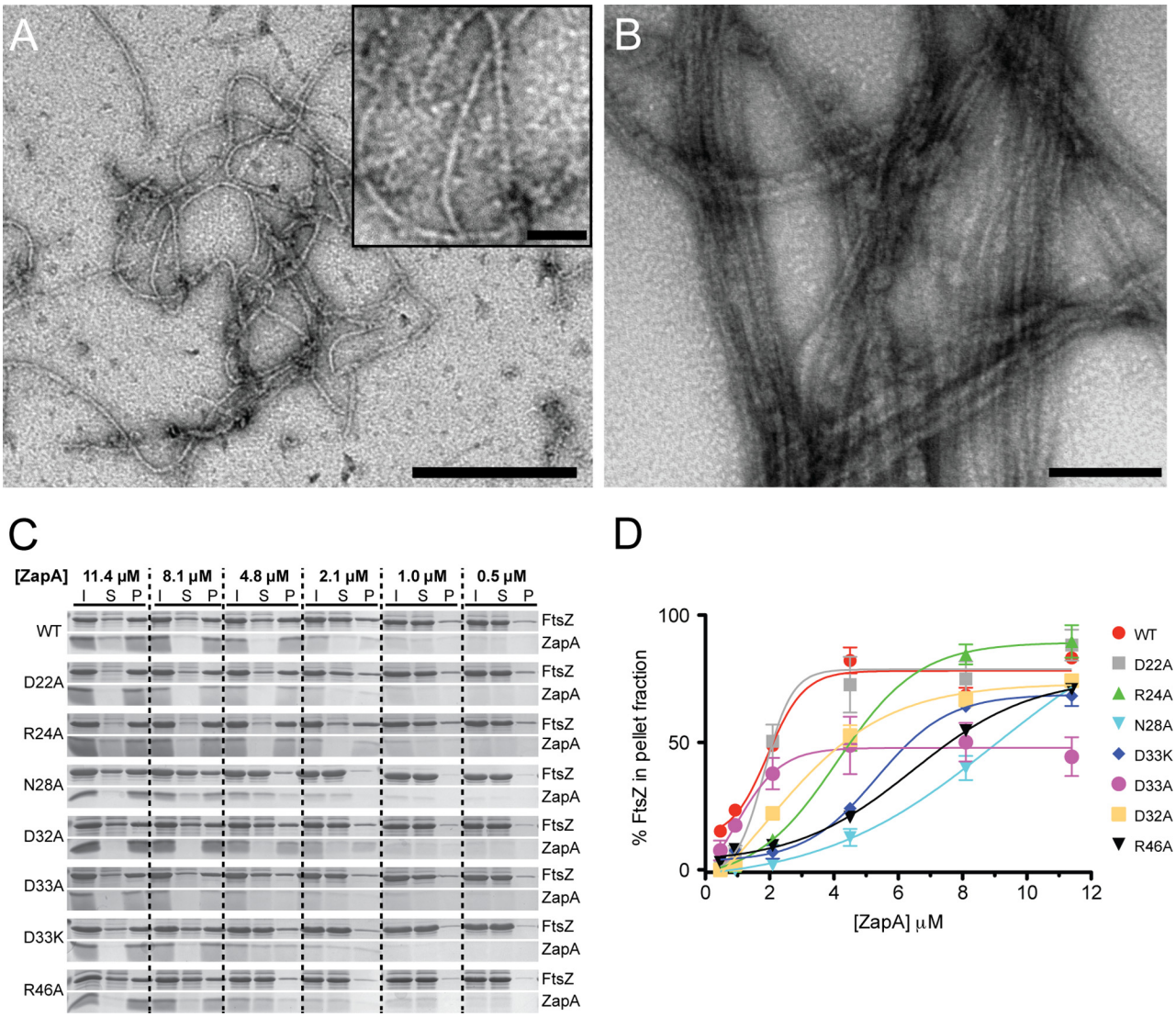

FIGURE 2. **FtsZ sedimentation assay and the percent of FtsZ in the pelleted fractions.** *A*, purified FtsZ filamented with 1 mM GTP in the absence of ZapA (*bar*, 250 nm; *inset bar*, 25 nm). *B*, FtsZ filaments bundled with purified ZapA (4.8 μM; *bar*, 100 nm). *C*, FtsZ (4.8 μM) filamented with 1 mM GTP in the presence of WT ZapA or ZapA variants (0.5–11.4 μM). Initial samples (*I*) were used to assess the total protein content in each reaction. Soluble (*S*) and pelleted (*P*) fractions were separated by centrifugation at 10,000 rpm for 15 min, and all three samples (*I*, *S*, and *P*) were analyzed by Coomassie-stained SDS-PAGE. Pelleted fractions contain FtsZ filaments that were bundled with ZapA. *D*, triplicate FtsZ sedimentation assays were performed for each ZapA variant, and Coomassie-stained SDS-PAGE results were analyzed by densitometry. The mean percentages of FtsZ in the pelleted fractions were plotted for each concentration of ZapA, where the *error bars* indicate ± S.E. (standard error of the mean). Reactions with equimolar ZapA (4.8 μM) and FtsZ (4.8 μM), lacking GTP, were run as a control for protein precipitation (not shown), and these values were subtracted from the sedimentation of each reaction.

Based on the data from the sedimentation assays (Fig. 2*D*), EC_{50} values were calculated that correspond to the concentration of ZapA needed to sediment 50% of FtsZ filaments in each reaction (Table 3). An increase in EC_{50} signifies that more variant ZapA is required to effectively sediment FtsZ compared with WT and therefore suggests these ZapA variants bundle FtsZ filaments less efficiently. For WT ZapA and ZapA D22A, similar EC_{50} values of 2.22 and 2.67 μM were determined, respectively. Higher EC_{50} values than WT were obtained for ZapA variants R24A, N28A, D32A, D33A, D33K, and R46A (Table 3).

ZapA Variants Demonstrate Reduced Bundling of FtsZ Filaments—To directly assess the effect of ZapA variants on FtsZ filament bundling, ZapA-FtsZ complexes were visualized by TEM (Fig. 3*A*). Visualization of bundling was performed at

TABLE 3
Summary of interactions for ZapA variants with FtsZ filaments

ZapA variant	EC_{50}[a]	Max Sed.[b]	Filaments/bundle[c]	Cell length[d]
	μM			μm
WT	2.22	0.87	9.86 ± 0.76	2.65 ± 0.06
D22A	2.67	0.93	7.33 ± 0.49	2.81 ± 0.08
R24A	4.48	0.94	7.13 ± 0.76	2.96 ± 0.15
N28A	8.77	0.75	5.21 ± 0.19	3.77 ± 0.25
D32A	4.86	0.71	5.73 ± 0.29	3.74 ± 0.17
D33A	8.74	0.53	5.75 ± 0.38	3.66 ± 0.17
D33K	7.05	0.78	5.46 ± 0.29	3.70 ± 0.10
R46A	7.61	0.74	NA[e]	3.87 ± 0.20

[a] EC_{50}, concentration of ZapA needed to sediment 50% of FtsZ in each reaction.
[b] Max Sed., maximum proportion of FtsZ pelleted by each ZapA variant in the sedimentation assays.
[c] Determined from transmission electron micrographs (means ± S.E.).
[d] Values were measured from transmission electron micrographs (means ± S.E.). The mean cell length of Δ*zapA E. coli* is 3.52 μm.
[e] NA, data not available because no bundles were observed in transmission electron micrographs.

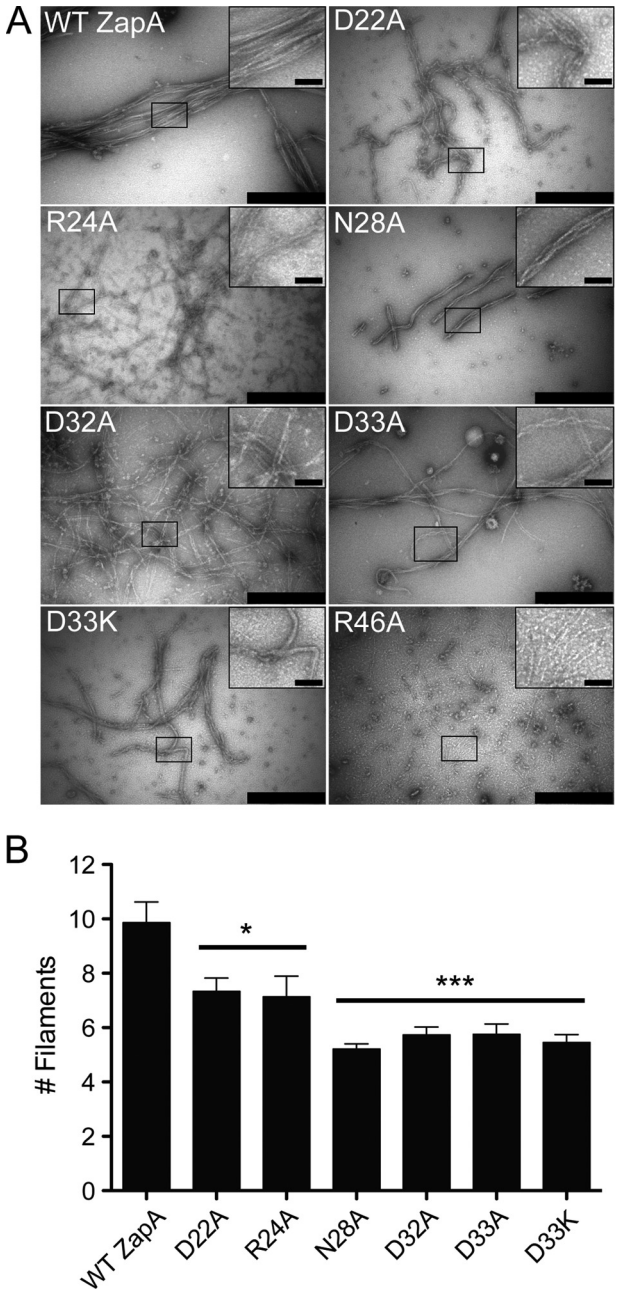

FIGURE 3. **Transmission electron microscopy reveals differential bundling of FtsZ filaments by ZapA variants.** *A*, equimolar concentrations of ZapA and FtsZ. FtsZ was filamented with 1 mM GTP and visualized by TEM (*bar*, 500 nm; *inset bar*, 50 nm). *B*, TEM images were analyzed, and the mean numbers of filaments per bundle ± S.E. were plotted for each ZapA variant ($n > 50$ bundles per ZapA variant); two-tailed *t* tests were used to compare ZapA variants to WT. *, $p < 0.05$; ***, $p < 0.0001$.

equimolar concentrations of ZapA and FtsZ, because this concentration revealed the greatest difference in FtsZ sedimentation between ZapA variants (Fig. 2*D*) and is also the most physiologically relevant (50). From these micrographs, the number of filaments within each bundle was determined (Fig. 3*B* and Table 3). A decrease in the number of FtsZ filaments per bundle would indicate a decreased ability of ZapA to bundle FtsZ. At equimolar concentrations (4.8 μM) WT ZapA-FtsZ filaments appear as long twisted bundles of laterally associated FtsZ filaments (Fig. 3*A*; WT), matching those described previously (14, 34, 46, 47) with an average of ~10 filaments per bundle (Fig. 3*B* and Table 3). FtsZ filaments bundled by ZapA variants D22A and R24A appeared less organized than those bundled by WT ZapA and demonstrated an average of ~7 filaments per bundle (Fig. 3*B* and Table 3). It should also be noted that bundles formed in the presence of R24A ZapA appeared to have fewer lateral associations and were less ordered (Fig. 3*A*). Electron micrographs also showed that ZapA N28A formed short twisted bundles of FtsZ filaments when compared with WT ZapA (Fig. 3*A*), whereas ZapA variants D32A, D33A, and D33K produced long, twisted bundles of FtsZ filaments similar to those formed by WT ZapA, although they still contained fewer (~5) FtsZ filaments per bundle (Fig. 3*B* and Table 3). Surprisingly, when sedimentation reactions containing ZapA variant R46A were imaged, no bundled FtsZ filaments, and very few nonbundled FtsZ filaments, were observed (Fig. 3*A*). This result was reproducible over six replicate experiments (data not shown). Based on the sedimentation profile of ZapA R46A, which is similar to that of WT ZapA (Fig. 2*D*), this suggests that the R46A variant may affect FtsZ polymer assembly or disassembly *in vitro*.

ZapA Variants That Demonstrate Reduced FtsZ Filament Bundling Are Unable to Generate Normal Cell Length in Vivo—To investigate the effect of the ZapA variants *in vivo*, a ZapA-deleted strain of *E. coli* (Δ*zapA*) was constructed. WT ZapA and ZapA variants were expressed in Δ*zapA E. coli*. No significant differences in growth were observed between any of these strains (Fig. 4*A*). Western blot analysis using an anti-His antibody confirmed that the His-tagged WT and ZapA variants were expressed at similar levels (Fig. 4*B*). The Δ*zapA E. coli* strain exhibited an elongated cell morphology as previously described (30), with a mean cell length of 3.52 μm (Fig. 4*C*). The WT ZapA variant restored a normal cell size with a mean cell length of 2.65 μm. As with the *in vitro* results, ZapA variants D22A and R24A restored cell length to that of WT ZapA, with mean cell lengths of 2.81 and 2.96 μm, respectively. However, ZapA variants N28A, D32A, D33A, D33K, and R46A did not restore Δ*zapA* cells to their normal length (Fig. 4*C* and Table 3). These results indicate that residues Asp^{22} and Arg^{24} are not critical for FtsZ bundling *in vivo*, whereas Asn^{28}, Asp^{32}, Asp^{33}, and Arg^{46} are needed to maintain the bundling function of ZapA.

The ability of this His-tagged ZapA protein to complement functionality *in vivo* is in contrast to a report by Mohammadi *et al.* (50) in which the addition of a His tag rendered ZapA nonfunctional *in vivo*. One notable difference between this construct and the one described previously is the cleavage site between the His tag and ZapA. The factor XA cleavage site used in this study contains fewer charged amino acids than the enterokinase cleavage site used by Mohammadi *et al.* (two *versus* five, respectively) (50). This could account for the differences seen in the *in vivo* and *in vitro* analyses of these proteins.

Immunofluorescence was also performed on these cells to monitor Z-ring formation and nucleoid segregation in Δ*zapA* cells carrying ZapA variants (Fig. 4*D*). WT *E. coli* cells divide normally, presenting a single condensed mid-cell localization of FtsZ and two segregated nucleoids destined for each of the

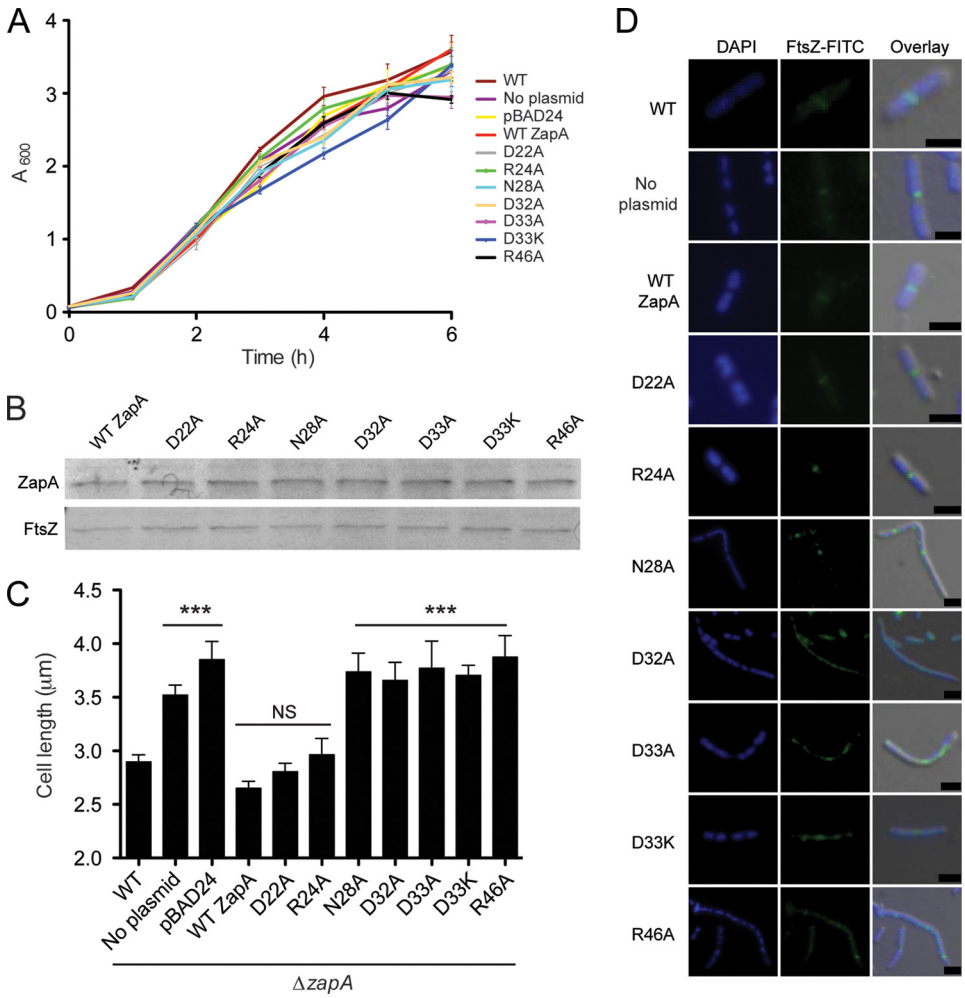

FIGURE 4. **Complementation of Δ*zapA* with WT ZapA and ZapA variants.** *E. coli* Δ*zapA* cells were transformed with pBAD24 carrying *zapA* variants. *A*, growth was monitored over 6 h, and no significant differences were observed in cell density. *B*, Western blot analysis using an anti-His antibody confirmed that ZapA variants were expressed to the same levels during the complementation assays in Δ*zapA* cells (*top panel*) and Western blot analysis using an anti-FtsZ antibody (*bottom panel*) was performed as a loading control for comparison. *C*, cells were visualized by TEM and measured ($n > 100$ cells per *E. coli* strain). Mean cell length values ± S.E. were plotted and analyzed by two-tailed *t* tests as compared with WT cell lengths. *NS*, no significant difference; ***, $p < 0.001$. No significant differences in cell length were observed between WT cells and WT ZapA complemented cells and between Δ*zapA* and pBAD24 vector control cells. *D*, immunofluorescence was performed to detect differences in FtsZ localization and Z-ring formation among WT cells and Δ*zapA* cells expressing WT ZapA and ZapA variants. *Scale*, 1 μm.

daughter cells (Fig. 4*D*, *top row*). The Δ*zapA* cells differ from WT *E. coli* in that elongated cells show multiple localizations of FtsZ and multiple nucleoids. When Δ*zapA* cells were complemented with WT ZapA and ZapA variants, D22A and R24A closely resemble WT *E. coli*. These variants show normal Z-rings and efficient cell division, indicated by a maximum of two nucleoids in each dividing cell. However, when Δ*zapA* cells were complemented with ZapA variants N28A, D32A, D33A, D33K, and R46A, elongated *E. coli* cells show multiple Z-rings and multiple nucleoids. Additionally, Z-rings in these cells often appeared diffuse, perhaps indicating less FtsZ bundling *in vivo*. Alternately, the diffuse localization pattern of FtsZ may be the result of an inability of these ZapA variants to properly align FtsZ at mid-cell via interactions with ZapB (30). Although these results are consistent with inefficient cell division, the phenotype is resolved by the late exponential phase, suggesting a delay in bacterial cell division as seen previously by Galli and Gerdes (37).

DISCUSSION

ZapA is proposed to stabilize FtsZ filaments, aiding in Z-ring formation and/or positioning prior to bacterial cell division (30, 36, 38–40, 50). Although ZapA alone is not essential for cell division, it is hypothesized that collectively ZapA, ZapB, ZapC, and ZapD are required for FtsZ filament bundling and dynamics in *E. coli* (14–18, 20). Although the ZapA protein is widely conserved across bacterial species, it is not required for the lateral association of FtsZ filaments in some organisms (51). In *E. coli* and *Bacillus subtilis*, ZapA has been shown to be important for FtsZ bundling *in vitro* (27), and the absence of ZapA results in an elongated cell phenotype and abnormal septum formation in *E. coli* cells (14, 30).

Although nearly a decade has passed since the crystallographic structure of ZapA from *P. aeruginosa* was determined and its role in FtsZ bundling was proposed (38), questions remain about the specificity of ZapA-FtsZ interactions and the implication of these interactions on Z-ring architecture and

dynamics. The structure of *Ec*ZapA should prove helpful in investigating these questions, given that *E. coli* has become the most common model for these studies. Although *Pa*ZapA has been used to probe the function and physiological role of ZapA in *E. coli* (40, 50), the details of the structure of *Ec*ZapA differ enough to impact the design and interpretation of ZapA structure-function studies. For example, a recent study by Pacheco-Gómez *et al.* (40) based their mutational analysis of the tetramerization domain of ZapA on the *Pa*ZapA structure, with the hypothesis that ZapA dimer/tetramer equilibrium is important for proper FtsZ bundling. Although they succeeded in making a properly folded ZapA dimer, Ile^{83} packs in a very different fashion in *Ec*ZapA than the equivalent residue in *Pa*ZapA, meaning that detailed predictions of the consequences of altering this residue are likely to be inaccurate. Interestingly, the I83E dimer variant of *Ec*ZapA interacted with FtsZ but did not form FtsZ bundled filaments *in vitro* (40). Given (i) the extensive stabilizing interactions within the *Ec*ZapA tetramer (Fig. 1*D*) and (ii) the predominant tetrameric configuration reported for WT ZapA by sedimentation velocity experiments (40), it is unlikely that native *Ec*ZapA dimers are present in sufficient levels to bundle FtsZ, as suggested for *Pa*ZapA (38). Therefore, *Ec*ZapA likely functions as a tetramer. If the N-terminal domains at both ends of the tetramer need to engage with FtsZ filaments to bundle them, the large observed differences in the orientation of these domains (Fig. 1, *D* and *E*) suggest differences in FtsZ bundling between these two species.

Here, the structure of *Ec*ZapA (Fig. 1) was used to better understand the role of ZapA in bundling and stabilizing FtsZ prior to bacterial cell division. Galli and Gerdes (36) recently showed that a 26-amino acid region of ZapA from *E. coli* was involved in ZapA-FtsZ interactions. In *Ec*ZapA, this region forms a charged α-helix (Fig. 1, *A* and *C*). Because this globular head of ZapA is not well conserved compared with the C-terminal tetramerization domain, and ZapA-FtsZ interactions vary in importance and extent between species (27), it is possible that this region may be critical for ZapA-FtsZ interactions in *E. coli*. Site-directed mutagenesis was used to create point mutations to alter specific amino acids along this charged α-helix. The functional implications of these point mutations at each residue are described in Fig. 5. ZapA variants at residues Asp^{22} and Arg^{24} (Fig. 5, *green*) show only minor deviations from WT ZapA-FtsZ interactions. ZapA R24A does not cause a significant change in FtsZ sedimentation at saturating concentrations (Fig. 2*D*), and this ZapA variant complemented the Δ*zapA* strain with the same efficiency as WT ZapA (Fig. 4). These results suggest that ZapA R24A interacts with FtsZ filaments. However, upon visualizing FtsZ filaments bundled by ZapA R24A, it became clear that the ZapA-FtsZ interactions were somewhat altered, because bundles appear as disorganized tangles of filaments as opposed to the laterally organized structures seen with WT ZapA (compare Fig. 3*A* WT *versus* R24A). Because the R24A ZapA variant appears to interact with FtsZ *in vitro* and *in vivo*, there are two possible explanations for this difference. First, ZapA R24A may have an altered functionality made possible by the removal of a charged residue involved in electrostatic interactions with FtsZ. Second, it is possible the full complementation of the Δ*zapA* phenotype

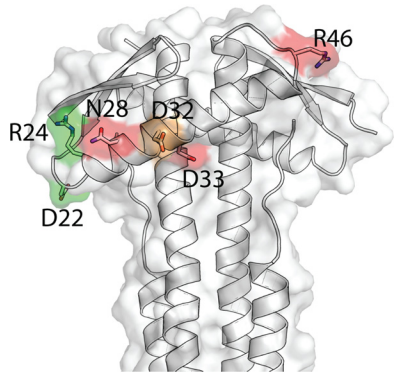

FIGURE 5. **Mutant phenotypes mapped onto the *Ec*ZapA structure.** Orientation as in Fig. 1*C*, but here colored according to the effect of point mutations at each residue. Residues in *green* have a relatively weak (though measurable) effect on the EC_{50} ($EC_{50} < 5$ μM), the number of filaments per bundle (>7) and the cell length (<3 μm). Residues highlighted in *red*, in contrast, have strong effects on the EC_{50} ($EC_{50} > 5$ μM), the number of filaments per bundle (<7), and the cell length (>3 μm). The residue highlighted in *orange* has a weak affect on the EC_{50} (EC_{50} <5) but nevertheless strongly affects both the number of filaments per bundle (<7) and the cell length (>3 μm).

in vivo is a result of the overlapping function of Zap proteins in *E. coli* (51).

ZapA variants with point mutations in the charged α-helix region at residues Asn^{28}, Asp^{33}, and Arg^{46} (Fig. 5, *red*) required much more ZapA to effectively bundle FtsZ filaments (Fig. 2*D*), demonstrated fewer FtsZ filaments per bundle (Fig. 3*B* and Table 3), and increased cell length in complementation assays (Fig. 4 and Table 3). In sedimentation assays, all of these ZapA variants demonstrated a significant decrease in FtsZ sedimentation at equimolar ($p < 0.02$) and saturated ($p < 0.05$) concentrations (Fig. 2*C*), and we linked this decrease in sedimentation to fewer FtsZ filaments per bundle (Fig. 3). It is also worth noting that these bundles appear to have adopted an inherent twisted, helical-like conformation, especially when observed as bundles of four FtsZ filaments. It cannot be determined whether this shift in conformation is a result of altered ZapA binding or whether it is a conformation typically seen with lower order FtsZ bundles. For ZapA variant R46A, we note that in the sedimentation assay FtsZ sediments significantly when ZapA is present at a saturating concentration (11.4 μM) (Fig. 2*C*). This contradicts the TEM results, where no significant bundling was observed (Fig. 3*A*). We hypothesize that this is due to a loss of bundling functionality, where ZapA may still be binding FtsZ filaments but in an altered way that does not allow the formation of organized, regularly spaced bundles. This may have functional implications for residue Arg^{46} in the coordination of ZapA in the FtsZ-ZapA interaction.

Interestingly, the D32A ZapA variant (Fig. 5, *orange*) presented only a weak effect on the measured EC_{50} values but strongly affected both the number of FtsZ filaments per bundle and the complemented cell length, suggesting that this residue may be important for enhancing Z-ring stability. Together, our results strongly suggest that the surface-exposed, charged residues on the *Ec*ZapA N-terminal α-helix mediate ZapA-FtsZ interactions to facilitate FtsZ filament bundling and Z-ring stability in dividing bacterial cells. Although this area of ZapA had been previously implicated in facilitating the ZapA-FtsZ interaction, this is the first report describing the structure of *Ec*ZapA

and the effects of altering specific residues in this region on the interaction with FtsZ.

Acknowledgments—We thank Chris Whitfield and Deborah Stewart Khursigara for critical reading of the manuscript and editorial assistance. X-ray data for EcZapA was collected at Canadian Light Source by Shaun Labiuk.

REFERENCES

1. Ward, J. E., Jr., and Lutkenhaus, J. (1985) Overproduction of FtsZ induces minicell formation in *E. coli*. *Cell* **42,** 941–949
2. Bi, E. F., and Lutkenhaus, J. (1991) FtsZ ring structure associated with division in *Escherichia coli*. *Nature* **354,** 161–164
3. Mukherjee, A., Dai, K., and Lutkenhaus, J. (1993) *Escherichia coli* cell division protein FtsZ is a guanine nucleotide binding protein. *Proc. Natl. Acad. Sci. U.S.A.* **90,** 1053–1057
4. Vicente, M., and Errington, J. (1996) Structure, function and controls in microbial division. *Mol. Microbiol.* **20,** 1–7
5. Bramhill, D., and Thompson, C. M. (1994) GTP-dependent polymerization of *Escherichia coli* FtsZ protein to form tubules. *Proc. Natl. Acad. Sci. U.S.A.* **91,** 5813–5817
6. Mukherjee, A., and Lutkenhaus, J. (1998) Dynamic assembly of FtsZ regulated by GTP hydrolysis. *EMBO J.* **17,** 462–469
7. Buddelmeijer, N., and Beckwith, J. (2002) Assembly of cell division proteins at the *E. coli* cell center. *Curr. Opin. Microbiol.* **5,** 553–557
8. Goehring, N. W., and Beckwith, J. (2005) Diverse paths to midcell: assembly of the bacterial cell division machinery. *Curr. Biol.* **15,** R514–R526
9. Natale, P., Pazos, M., and Vicente, M. (2013) The *Escherichia coli* divisome: born to divide. *Environ. Microbiol.* **15,** 3169–3182
10. Wang, X., Possoz, C., and Sherratt, D. J. (2005) Dancing around the divisome: asymmetric chromosome segregation in *Escherichia coli*. *Genes Dev.* **19,** 2367–2377
11. Aarsman, M. E., Piette, A., Fraipont, C., Vinkenvleugel, T. M., Nguyen-Distèche, M., and den Blaauwen, T. (2005) Maturation of the *Escherichia coli* divisome occurs in two steps. *Mol. Microbiol.* **55,** 1631–1645
12. de Boer, P. A. (2010) Advances in understanding *E. coli* cell fission. *Curr. Opin. Microbiol.* **13,** 730–737
13. Vicente, M., and Rico, A. I. (2006) The order of the ring: assembly of *Escherichia coli* cell division components. *Mol. Microbiol.* **61,** 5–8
14. Gueiros-Filho, F. J., and Losick, R. (2002) A widely conserved bacterial cell division protein that promotes assembly of the tubulin-like protein FtsZ. *Genes Dev.* **16,** 2544–2556
15. Ebersbach, G., Galli, E., Møller-Jensen, J., Löwe, J., and Gerdes, K. (2008) Novel coiled-coil cell division factor ZapB stimulates Z ring assembly and cell division. *Mol. Microbiol.* **68,** 720–735
16. Hale, C. A., Shiomi, D., Liu, B., Bernhardt, T. G., Margolin, W., Niki, H., and de Boer, P. A. (2011) Identification of *Escherichia coli* ZapC (YcbW) as a component of the division apparatus that binds and bundles FtsZ polymers. *J. Bacteriol.* **193,** 1393–1404
17. Durand-Heredia, J. M., Yu, H. H., De Carlo, S., Lesser, C. F., and Janakiraman, A. (2011) Identification and characterization of ZapC, a stabilizer of the FtsZ ring in *Escherichia coli*. *J. Bacteriol.* **193,** 1405–1413
18. Durand-Heredia, J., Rivkin, E., Fan, G., Morales, J., and Janakiraman, A. (2012) Identification of ZapD as a cell division factor that promotes the assembly of FtsZ in *Escherichia coli*. *J. Bacteriol.* **194,** 3189–3198
19. Rico, A. I., Krupka, M., and Vicente, M. (2013) In the beginning, *Escherichia coli* assembled the proto-ring: an initial phase of division. *J. Biol. Chem.* **288,** 20830–20836
20. Huang, K.-H., Durand-Heredia, J., and Janakiraman, A. (2013) FtsZ ring stability: of bundles, tubules, crosslinks, and curves. *J. Bacteriol.* **195,** 1859–1868
21. Popp, D., Iwasa, M., Narita, A., Erickson, H. P., and Maéda, Y. (2009) FtsZ condensates: an *in vitro* electron microscopy study. *Biopolymers.* **91,** 340–350
22. Osawa, M., Anderson, D. E., and Erickson, H. P. (2009) Curved FtsZ protofilaments generate bending forces on liposome membranes. *EMBO J.* **28,** 3476–3484
23. Rivas, G., López, A., Mingorance, J., Ferrándiz, M. J., Zorrilla, S., Minton, A. P., Vicente, M., and Andreu, J. M. (2000) Magnesium-induced linear self-association of the FtsZ bacterial cell division protein monomer: the primary steps for FtsZ assembly. *J. Biol. Chem.* **275,** 11740–11749
24. Löwe, J., and Amos, L. A. (1999) Tubulin-like protofilaments in Ca^{2+}-induced FtsZ sheets. *EMBO J.* **18,** 2364–2371
25. Erickson, H. P., Taylor, D. W., Taylor, K. A., and Bramhill, D. (1996) Bacterial cell division protein FtsZ assembles into protofilament sheets and minirings, structural homologs of tubulin polymers. *Proc. Natl. Acad. Sci. U.S.A.* **93,** 519–523
26. Niu, L., and Yu, J. (2008) Investigating intracellular dynamics of FtsZ cytoskeleton with photoactivation single-molecule tracking. *Biophys. J.* **95,** 2009–2016
27. Anderson, D. E., Gueiros-Filho, F. J., and Erickson, H. P. (2004) Assembly dynamics of FtsZ rings in *Bacillus subtilis* and *Escherichia coli* and effects of FtsZ-regulating proteins. *J. Bacteriol.* **186,** 5775–5781
28. Thanedar, S., and Margolin, W. (2004) FtsZ exhibits rapid movement and oscillation waves in helix-like patterns in *Escherichia coli*. *Curr. Biol.* **14,** 1167–1173
29. Li, Z., Trimble, M. J., Brun, Y. V., and Jensen, G. J. (2007) The structure of FtsZ filaments *in vivo* suggests a force-generating role in cell division. *EMBO J.* **26,** 4694–4708
30. Buss, J., Coltharp, C., Huang, T., Pohlmeyer, C., Wang, S.-C., Hatem, C., and Xiao, J. (2013) *In vivo* organization of the FtsZ-ring by ZapA and ZapB revealed by quantitative super-resolution microscopy. *Mol. Microbiol.* **89,** 1099–1120
31. Strauss, M. P., Liew, A. T., Turnbull, L., Whitchurch, C. B., Monahan, L. G., and Harry, E. J. (2012) 3D-SIM super resolution microscopy reveals a bead-like arrangement for FtsZ and the division machinery: implications for triggering cytokinesis. *PLoS Biol.* **10,** e1001389
32. Fu, G., Huang, T., Buss, J., Coltharp, C., Hensel, Z., and Xiao, J. (2010) *In vivo* structure of the *E. coli* FtsZ-ring revealed by photoactivated localization microscopy (PALM). *PLoS One* **5,** e12682
33. Biteen, J. S., Goley, E. D., Shapiro, L., and Moerner, W. E. (2012) Three-dimensional super-resolution imaging of the midplane protein FtsZ in live *Caulobacter crescentus* cells using astigmatism. *Chemphyschem.* **13,** 1007–1012
34. Holden, S. J., Pengo, T., Meibom, K. L., Fernandez Fernandez, C., Collier, J., and Manley, S. (2014) High throughput 3D super-resolution microscopy reveals *Caulobacter crescentus in vivo* Z-ring organization. *Proc. Natl. Acad. Sci. U.S.A.* **111,** 4566–4571
35. Monahan, L. G., Robinson, A., and Harry, E. J. (2009) Lateral FtsZ association and the assembly of the cytokinetic Z ring in bacteria. *Mol. Microbiol.* **74,** 1004–1017
36. Galli, E., and Gerdes, K. (2012) FtsZ-ZapA-ZapB interactome of *Escherichia coli*. *J. Bacteriol.* **194,** 292–302
37. Galli, E., and Gerdes, K. (2010) Spatial resolution of two bacterial cell division proteins: ZapA recruits ZapB to the inner face of the Z-ring. *Mol. Microbiol.* **76,** 1514–1526
38. Low, H. H., Moncrieffe, M. C., and Löwe, J. (2004) The crystal structure of ZapA and its modulation of FtsZ polymerisation. *J. Mol. Biol.* **341,** 839–852
39. Small, E., Marrington, R., Rodger, A., Scott, D. J., Sloan, K., Roper, D., Dafforn, T. R., and Addinall, S. G. (2007) FtsZ polymer-bundling by the *Escherichia coli* ZapA orthologue, YgfE, involves a conformational change in bound GTP. *J. Mol. Biol.* **369,** 210–221
40. Pacheco-Gómez, R., Cheng, X., Hicks, M. R., Smith, C. J., Roper, D. I., Addinall, S., Rodger, A., and Dafforn, T. R. (2013) Tetramerization of ZapA is required for FtsZ bundling. *Biochem. J.* **449,** 795–802
41. Larkin, M. A., Blackshields, G., Brown, N. P., Chenna, R., McGettigan, P. A., McWilliam, H., Valentin, F., Wallace, I. M., Wilm, A., Lopez, R., Thompson, J. D., Gibson, T. J., and Higgins, D. G. (2007) Clustal W and Clustal X version 2.0. *Bioinformatics.* **23,** 2947–2948
42. Datsenko, K. A., and Wanner, B. L. (2000) One-step inactivation of chromosomal genes in *Escherichia coli* K-12 using PCR products. *Proc. Natl. Acad. Sci. U.S.A.* **97,** 6640–6645
43. Datta, S., Costantino, N., and Court, D. L. (2006) A set of recombineering plasmids for gram-negative bacteria. *Gene.* **379,** 109–115

44. Kabsch, W. (2010) XDS. *Acta Crystallogr. D Biol. Crystallogr.* **66,** 125–132
45. McCoy, A. J., Grosse-Kunstleve, R. W., Adams, P. D., Winn, M. D., Storoni, L. C., and Read, R. J. (2007) Phaser crystallographic software. *J. Appl. Crystallogr.* **40,** 658–674
46. Adams, P. D., Grosse-Kunstleve, R. W., Hung, L.-W., Ioerger, T. R., McCoy, A. J., Moriarty, N. W., Read, R. J., Sacchettini, J. C., Sauter, N. K., and Terwilliger, T. C. (2002) PHENIX: building new software for automated crystallographic structure determination. *Acta Crystallogr. D Biol. Crystallogr.* **58,** 1948–1954
47. Emsley, P., and Cowtan, K. (2004) Coot: model-building tools for molecular graphics. *Acta Crystallogr. D Biol. Crystallogr.* **60,** 2126–2132
48. Schneider, C. A., Rasband, W. S., and Eliceiri, K. W. (2012) NIH Image to ImageJ: 25 years of image analysis. *Nat. Methods* **9,** 671–675
49. Hiraga, S., Ichinose, C., Niki, H., and Yamazoe, M. (1998) Cell cycle-dependent duplication and bidirectional migration of SeqA-associated DNA-protein complexes in *E. coli*. *Mol. Cell.* **1,** 381–387
50. Mohammadi, T., Ploeger, G. E., Verheul, J., Comvalius, A. D., Martos, A., Alfonso, C., van Marle, J., Rivas, G., and den Blaauwen, T. (2009) The GTPase activity of *Escherichia coli* FtsZ determines the magnitude of the FtsZ polymer bundling by ZapA *in vitro*. *Biochemistry* **48,** 11056–11066
51. Dajkovic, A., Pichoff, S., Lutkenhaus, J., and Wirtz, D. (2010) Cross-linking FtsZ polymers into coherent Z rings. *Mol. Microbiol.* **78,** 651–668